Temperature-dependent scattering of hyperthermal energy K^+ ions

J. Powers* and J. R. Manson
Department of Physics and Astronomy, Clemson University, Clemson, South Carolina 29634, USA

C. E. Sosolik,† J. R. Hampton,‡ A. C. Lavery,§ and B. H. Cooper‖
Laboratory of Atomic and Solid State Physics, Cornell University, Ithaca, New York 14853-2501, USA
(Received 10 May 2004; published 20 September 2004)

Extensive experimental and theoretical results are presented for the scattering of a beam of K^+ ions incident on a Cu(001) surface along the ⟨100⟩ azimuth with incident energies of 50 to 154 eV. Energy-resolved scattered intensity spectra reveal three distinct peaks whose widths and intensities vary with surface temperature. Using the results of a classical trajectory simulation, four distinct ionic trajectory types are assigned to these peaks. Using a classical mechanical theory that contains the correct equilibrium thermodynamics of the Cu crystal, general features of the K^+ energy-resolved spectra are calculated for each trajectory type and compared with the experimental results. For the case of single ion-surface atom collisions, the dependence of the peak intensities and widths on the incident energy and surface temperature is well explained by the classical theory.

DOI: 10.1103/PhysRevB.70.115413 PACS number(s): 68.35.Ja, 68.49.Bc, 79.20.Rf, 03.65.Sq

I. INTRODUCTION

Experimental and theoretical studies that probe the scattering dynamics of hyperthermal energy (≈1 eV to 1 keV) ions with surfaces are important because they provide fundamental knowledge about ion-surface interactions.[1] Recent experiments, for example, have studied the dynamics of scattering, trapping, and charge transfer for hyperthermal energy alkali ions incident on metal surfaces.[2–9] The knowledge gained from this work can be applied to the many technological processes that rely on ion-surface scattering, such as ion-beam etching, desorption, and secondary ion mass spectrometry (SIMS).[10–12]

Few studies have focused on the role that surface temperature plays in the scattering process at hyperthermal energies.[2,3,6,13–15] Of those measurements, the most notable were aimed at demonstrating a sensitivity to the effects of surface dynamics and focused on the thermal broadening of peak widths in either energy-resolved or angular spectra. For example, Verhey *et al.*[13] and Poelsema *et al.*[14,15] measured the thermal broadening of peaks in the energy-resolved spectra of Kr^+ scattered from Cu(001). By comparing simulated and experimental results for the broadening of peaks due to a particular triple scattering trajectory, they were able to obtain a value for the surface Debye temperature. A more recent investigation focused on the scattering of Na^+ from Cu(001) as a function of surface temperature.[2] In this work, DiRubio *et al.* demonstrated that experimentally observed backscattered ion distributions fail to be described by simple theoretical models, such as the trajectory approximation. A completely classical scattering theory, however, that includes both the recoil and thermodynamics of the Cu(001) target, has been shown to provide a reasonable description of scattering processes in this energy range.[2,16]

In this paper, we examine a series of experiments involving K^+ scattering from Cu(001) with incident energies between 50 and 154 eV. Energy-resolved spectra of scattered ions obtained as a function of the surface temperature are compared with a classical scattering theory.[16] Our measurements are not sensitive to the thermal charge transfer effects that can arise for Na^+ beams.[9] Therefore, unlike the Na^+ measurements made by DiRubio *et al.*,[2] we obtain relative scattering intensities for the K^+ as a function of surface temperature. From these data, theoretically predicted temperature-dependences of the widths, intensities, and integrated intensities of the peaks are tested.

This paper is organized in the following manner. In Sec. II, we describe the experimental apparatus and techniques used to obtain the K^+ scattering data. The classical scattering theory used to model these data is discussed in Sec. III. In Sec. IV, the experimental data and theoretical calculations are presented and compared. Finally, in Sec. V, we summarize our results and present some overall conclusions that one can draw from this work.

II. EXPERIMENT

The data presented here were obtained in an ultra high vacuum (UHV) chamber and beamline described in detail elsewhere.[17–19] The K^+ beams were produced in a Colutron ion source which has been modified to allow efficient production of alkali ions from commercially available solid state ion sources.[20–22] Beams produced by this source are typically Gaussian in shape with a size of 0.8 mm (FWHM).[23] The incident beams were directed along the ⟨100⟩ azimuth of a Cu(001) single crystal at an incident angle of 45° from the surface normal. Using low energy electron diffraction (LEED), the ⟨100⟩ azimuth of the sample was aligned to within ±2° of the incident ion beam direction. This alignment was fine-tuned to within ±0.5° by monitoring the scattered ion beam intensity, which is highly sensitive to the azimuthal orientation. The sample was cleaned by repeated cycles of 500 eV Ar^+ sputtering followed by anneals at 600 °C. The cleanliness and order of the sample were moni-

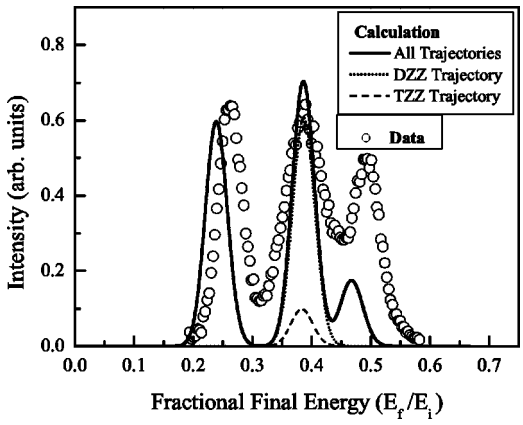

FIG. 1. Energy-resolved intensity spectra as a function of the fractional final energy at the incident energy $E_i = 154$ eV and temperature $T_S = 675$ K. The experimental data are shown as points. The solid curve is the sum of contributions from the four trajectories discussed in Sec. III of the text. The leftmost and rightmost peaks correspond to the SS and DF trajectories, respectively. The middle peak contains both DZZ (dashed curve) and TZZ (dotted curve) contributions.

tored by Auger electron spectroscopy and LEED, respectively.

Energy-resolved spectra of the scattered K^+ were measured with an electrostatic analyzer (ESA) at a final angle of 45° from the surface normal for incident K^+ energies of 50, 99, and 154 eV. The ESA has an energy resolution of $\Delta E/E = 0.016$ and an effective angular acceptance of approximately ±0.5°. For each incident energy, the temperature of the Cu(001) sample, T_S, was varied between approximately 325 and 925 K. This variation in temperature, which was monitored with a Chromel-Alumel thermocouple, was achieved using a combination of cooling from a liquid nitrogen reservoir connected by copper braids and heating from an electron-beam heater mounted behind the sample. Measurements made using a neutral particle detector[24] have shown that neutralization effects at these incident energies and sample temperatures are small, typically less than ~1.5%.[25–27] Therefore, no corrections for neutralization were included in the data presented in this paper.

A typical spectrum obtained for K^+ is shown in Fig. 1. This spectrum and all other spectra of scattered ions presented in this paper consist primarily of three broad but distinct peaks. The trajectories that contribute to the peaks in the spectra were previously identified, through comparisons with classical trajectory simulations,[2,28,30] as the result of four well-defined scattering paths: (1) Single scattering directly from one Cu atom (SS); (2) double forward scattering (DF), in which the ion collides with a Cu atom and then moves forward nearly parallel to the surface and suffers a second collision with the next nearest neighbor ⟨100⟩ Cu atom;[31] (3) double zig-zag scattering (DZZ), in which the second collision is with the next forward nearest neighbor in the adjacent ⟨100⟩ row; and (4) triple zig-zag scattering (TZZ), which consists of the two collisions of the DZZ trajectory (case 3 above) followed by a third collision with a Cu atom in the original ⟨100⟩ row. Ions following the DZZ and TZZ paths lose similar amounts of energy and form a single peak in the energy resolved spectra that cannot be distinguished as two separate processes. We refer to this combined peak as the multiple scattering (MS) peak. The spectra were fit to a sum of three Gaussians plus a small linear background term. The peak positions, intensities, and widths extracted from these fits were then compared to the results obtained from the classical scattering theory discussed in the next section.

III. THEORETICAL MODEL

In this section we review the theoretical model that we have used to describe our K^+ experimental results. Our model is similar to that employed in previous work on Na^+ and rare gas scattering from Cu(001) and molten metal surfaces.[16,32,33] This particular theoretical treatment provides simple closed-form analytic expressions for scattering events in terms of differential reflection coefficients. As we discuss below, multiple reflection coefficients can be convolved, allowing us to model relatively complex scattering events, such as the TZZ and DZZ scattering trajectories described in Sec. II. Here we describe the reflection coefficients and discuss the parameters we have used to model our experimental data. Also, we outline the predicted temperature-dependence of the widths, intensities, and integrated intensities of peaks in the scattered spectra.

A trajectory that involves the single collision scattering of an atom-like projectile from a surface at temperature T_S can be described in terms of the differential reflection coefficient, $dR^{(1)}/d\Omega_f dE_f$, which gives the fraction of particles scattered into the solid angle $d\Omega_f$ and energy range dE_f centered at Ω_f and E_f. This coefficient is given by[16,34]

$$\frac{dR^{(1)}(\mathbf{p}_f,\mathbf{p}_i)}{d\Omega_f dE_f} = \frac{m^2|\mathbf{p}_f|}{8\pi^3\hbar^4 p_{iz}}|\tau_{fi}|^2\left(\frac{\pi}{\Delta E_0 k_B T_S}\right)^{1/2} \times \exp\left\{-\frac{(\Delta E+\Delta E_0)^2}{4k_B T_S \Delta E_0}\right\}, \quad (1)$$

where $\Delta E = E_f - E_i$ is the difference between the final and initial projectile energies, $|\tau_{fi}|^2$ is the scattering form factor of a unit cell, m is the projectile mass, and the momentum $\mathbf{p}_q$ of a particle in state q is divided into components $(\mathbf{P}_q, p_{qz})$ parallel and perpendicular to the surface, respectively. The recoil energy shift is $\Delta E_0 = (\mathbf{p}_f - \mathbf{p}_i)^2/2M_c$, where M_c is the mass of an atom in the crystal. The differential reflection coefficient given by Eq. (1) is appropriate for K^+ scattering in the hyperthermal regime, as it describes the scattering of the incident atomic projectile with a surface made up of discrete scattering centers that are initially in thermodynamic equilibrium. Other forms of this reflection coefficient, appropriate for scattering from corrugated and flat-repulsive surfaces, have also been obtained.[16,32,35]

More complex scattering trajectories, involving successive collisions with different target atoms, can be written as a convolution of the corresponding single-particle collisions. For instance, the contribution to the differential reflection coefficient arising from double scattering is expressed as

$$\frac{dR^{(2)}(\mathbf{p}_f,\mathbf{p}_i)}{d\Omega_f dE_f} = \sum_{n=1}^{N} \int_0^\infty dE_q \int_{\Delta\Omega_n} d\Omega_q \frac{dR^{(1)}(\mathbf{p}_f,\mathbf{p}_q)}{d\Omega_f dE_f} \frac{dR^{(1)}(\mathbf{p}_q,\mathbf{p}_i)}{d\Omega_q dE_q}, \tag{2}$$

where the summation is over the set of target atoms with which second collisions can occur and $\Delta\Omega_n$ is the solid angle subtended by the classical cross section of the nth atom. Third order scattering events can be similarly written as a double convolution over a product of three single scattering terms.[32] To accurately describe our data for K^+ scattering, we must account for the four trajectory types described in Sec. II. Therefore, the total differential reflection coefficient used in this work is the sum of the single and double scattering terms of Eqs. (1) and (2) plus a triple scattering term.

In addition to describing K^+ scattering trajectories in terms of the differential reflection coefficients discussed above, we have also made several simplifications which are noted here. First, we take the form factor $|\tau_{fi}|^2$ to be constant, which is appropriate for classical hard sphere scattering.[32] Additionally, since the solid angles subtended by the target atoms in the second and third collisions of the DF, DZZ, and TZZ trajectories are small, we assume that the angular dependence of the intermediate differential reflection coefficients can be ignored. Therefore, the angular integration can be replaced by a multiplicative factor of $\Delta\Omega_n$. For DF scattering in the $\langle 100\rangle$ surface azimuth, the classical cross-section of the target atom, $\Delta\Omega$, is the solid angle subtended by the cross-section of a Cu atom at the lattice spacing distance of $a=3.61$ Å. The simplest approximation for $\Delta\Omega/4\pi$ is the ratio of the Cu cross section to the area of a sphere of radius a, and based on the Cu atomic radius of 1.57 Å or covalent radius of 1.17 Å this implies expected values of $\Delta\Omega/4\pi$ for DF trajectories that lie between 0.047 and 0.026, respectively. For the DZZ and TZZ trajectories, which involve excursions out of the scattering plane, $\Delta\Omega$ is consequently larger by a factor of 2, due to the smaller nearest-neighbor distance between successive surface Cu atoms. For all calculations in this paper, the value of $\Delta\Omega/4\pi$ for DF collisions was chosen to be 0.031 corresponding to a Cu radius of 1.28 Å which lies between the accepted values for the covalent and atomic radii.

As we discussed above, trajectory analysis indicates that SS, DF, DZZ, and TZZ trajectories comprise the primary types that must be considered to describe our data. The SS trajectory is accounted for by Eq. (1) and depends on no adjustable parameters. DF trajectories, involving successive collisions with two nearest-neighbor surface atoms in the $\langle 100\rangle$ direction, depend on only one parameter, $\Delta\Omega$. DZZ trajectories involve next nearest neighbor particles in the forward $\langle 110\rangle$ direction and depend on an additional parameter, the intermediate scattering angle θ_{qD}. TZZ trajectories depend on two additional angular parameters, θ_{qT} and θ_{rT},[2,32,36] as they involve scattering from both a next nearest neighbor in the forward $\langle 110\rangle$ direction and a next nearest neighbor in the forward $\langle \overline{110}\rangle$ direction.

Values have been obtained for the additional DZZ and TZZ parameters using a classical trajectory simulation.[28,36] The trajectory simulation shows that these angles, listed in Table I, are larger for higher incident beam energies. All calculations were carried out using an average over the two naturally occurring stable isotopes of Cu, i.e., 69.17% of ^{63}Cu and 30.83% of ^{65}Cu as well as an average over the two stable isotopes of K, i.e., 93.26% of ^{39}K and 6.73% of ^{41}K. It should also be noted that the calculations presented here do not include effects of the attractive image potential. Independent ion scattering experiments have clearly demonstrated that for singly charged ion scattering on Cu surfaces, charge transfer and ion neutralization are negligible effects at the energies and surface temperatures considered here.[25–27] Therefore, the projectile will remain singly charged throughout the scattering trajectory and will be affected by the image potential. However, using our classical trajectory simulation, we have observed that the effects of a typical surface image potential well ($\sim$1–2 eV) on scattering at the incident energies considered here are negligible.[29]

TABLE I. Values for the intermediate scattering angles at each of the three measured energies, determined by trajectory simulation and given in degrees.

	50 eV	99 eV	154 eV
θ_{qD}	20.0	23.5	25.5
θ_{qT}	8.5	13.0	15.5
θ_{rT}	7.0	10.5	12.0

For hyperthermal incident energies and small mass ratios ($\mu=m/M_c<1$), such as the case we are dealing with here, the differential reflection coefficient of Eq. (1) is nearly Gaussian in shape and the characteristics of the scattered intensity are straightforward to describe. The calculated most probable energy (peak position) of Eq. (1) is approximately the zero of the argument of the exponential, $\overline{E_f}=E_i-\Delta E_0(\overline{E_f})$, which can be expressed as the familiar Baule formula for energy transfer in a collision of two point particles, $\overline{E_f}=f(\theta)E_i$, where θ is the total scattering angle (the angle between $\mathbf{p}_i$ and $\mathbf{p}_f$) and

$$f(\theta) = \left(\frac{\sqrt{1-\mu^2\sin^2\theta}+\mu\cos\theta}{1+\mu}\right)^2. \tag{3}$$

The width of the Gaussian-like distribution, expressed as the mean square deviation $\langle \Delta E^2\rangle$ from $\overline{E_f}$ is

$$\langle \Delta E^2\rangle \approx 2g(\theta)E_i k_B T_S, \tag{4}$$

where

$$g(\theta) = \frac{g_{TA}(\theta)}{(1+\mu-\mu\cos\theta/\sqrt{f(\theta)})} \tag{5}$$

and

$$g_{TA}(\theta) = \mu(1+f(\theta)-2\sqrt{f(\theta)}\cos\theta), \tag{6}$$

is the value taken by $g(\theta)$ in the trajectory approximation. Equation (6) is defined by

$$\Delta E_0(\overline{E_f}) = g_{TA}(\theta)E_i, \tag{7}$$

which demonstrates that the trajectory approximation is contained within Eq. (1) if one assumes that ΔE_0 appearing in the numerator (but not that in the denominator) of the argument of the exponential is a constant. The intensity at the point of most probable energy transfer, the peak intensity, is given by the envelope function, which appears as

$$I_{\max} \propto \frac{1}{(k_B T_S \Delta E_0)^{1/2}} \approx \frac{1}{(g_{TA}(\theta) k_B T_S E_i)^{1/2}}. \tag{8}$$

For fixed initial and final scattering angles, the width of the Gaussian-type distribution goes as $(E_i k_B T_S)^{1/2}$ as shown in Eq. (4) and the intensity from Eq. (8) goes as $(E_i k_B T_S)^{-1/2}$. Therefore, the integrated intensity of the single scattering peak should be independent of both temperature T_S and energy E_i. One should expect similar temperature dependences for the higher order scattering terms, as they are simply convolutions of the Gaussian-type single scattering term. In the next section, these temperature-dependent peak parameters, the width, intensity, and integrated intensity, are compared with our K^+ scattering results.

IV. COMPARISON OF THEORETICAL AND EXPERIMENTAL RESULTS

Using the experimental and theoretical techniques outlined in the previous two sections, we have investigated the scattering of K^+ ions from Cu(001) at incident energies of 50, 99, and 154 eV and sample temperatures between 325 and 925 K. In this section, we compare our experimental data and calculated results, focusing on the following features in the energy-resolved spectra: peak positions (Sec. IV A), peak intensities and widths (Sec. IV B), and integrated intensities (Sec. IV C).

A. Peak positions

A typical experimental and theoretical energy-resolved spectrum obtained for 154 eV K^+ at a surface temperature of 675 K is shown in Fig. 1. In the experimental spectrum one can see three peaks which arise from the different trajectory types discussed above. Using the trajectory simulation SAFARI,[28] we have determined the dominant trajectory types for these peaks to be, in order of increasing fractional final energy (E_f/E_i), the SS, MS, and DF at $E_f/E_i \approx 0.26$, 0.38, and 0.49, respectively. This particular ordering of the peaks with respect to energy is not surprising if one considers the trajectories and the collisions associated with them in terms of Eq. (3). Specifically, one finds that although the MS and DF trajectories involve more than one collision with Cu atoms, the scattering angle θ associated with each collision is small compared to that for the SS trajectory $(\theta = 90°)$. Therefore, the total energy loss for an MS or DF trajectory is less than what one obtains for a large scattering angle collision of the SS trajectory type. This result is completely accounted for by the classical scattering theory presented in Sec. III, and, as one can see in Fig. 1, the results of our theoretical calculations agree qualitatively with the experimental data.

To illustrate that both the DZZ and TZZ trajectory types are included in the MS peak at $E_f/E_i \approx 0.38$, the calculated contributions from these two trajectory types have been plotted separately in Fig. 1. One can see that the SS and DZZ trajectories have comparable intensities, while the TZZ trajectory has a smaller contribution that coincides in energy with the DZZ peak. This overlap between the DZZ and TZZ trajectory types makes it difficult to separate their individual contributions in the experimental data. Therefore, as we discussed in Sec. II, we refer to these two contributions as the MS peak. One should note that for all the calculations shown here and in successive figures, the results were normalized to the experimental data for each given incident energy at a surface temperature of 675 K.

The results shown in Fig. 1 demonstrate the qualitative agreement that we obtain between experiment and theory. They also show that there is a systematic difference in energy between the peak positions of the experimental and theoretical spectra. This difference is especially apparent for the simpler SS and DF trajectory types and has been observed at other incident energies and substrate temperatures. It is much less evident for the more complicated MS trajectories. Two possible sources for these differences are the image potential and the many-body nature of the ion-surface collision. The role of the image potential in K^+ scattering and in the present theoretical treatment was discussed in Sec. III. There we noted that the incident K^+ projectiles are expected to remain positively charged throughout their trajectories, which implies that the path the ions take near the surface will be affected by the image potential. However, when one examines the relative energy scales involved in the scattering, it is clear that the effects will be small, which is why we have chosen not to account for the image potential in our current calculations. Nevertheless, given the quantitative discrepancies observed in Fig. 1, it is reasonable to consider whether the image potential would bring these results into better agreement. It is well known that the effect of an attractive image potential is to refract the scattering ion toward the surface, i.e., towards smaller incident angles and larger outgoing angles. For the simplest case of scattering, the SS trajectory type, this image potential refraction will lead to a larger total scattering angle, which will give a greater energy loss and shift the calculated results of Fig. 1 further out of agreement. An alternative explanation for the reduced energy loss observed in the experimental data is the quasiness of the collisions between the K^+ ions and the Cu surface atoms. To be specific, the collisions can be more accurately represented as occuring between both the main collision partners discussed in Sec. II as well as between the scattering K^+ ion and a number of neighboring surface atoms. A detailed analysis of this effect was carried out using the trajectory simulation SAFARI, where it was shown that quasiness is in fact the most probable source of the reduced energy loss that is observed for K^+.[36]

We have accounted for the quasi-collisions between K^+ ions and the Cu surface in our calculations by assuming that the K^+ ions collide with an object that has an effective mass slightly larger than that of a single Cu surface atom. In Fig. 2, we compare the data of Fig. 1 as well as data for all other temperatures measured at $E_i = 154$ eV to calculated results

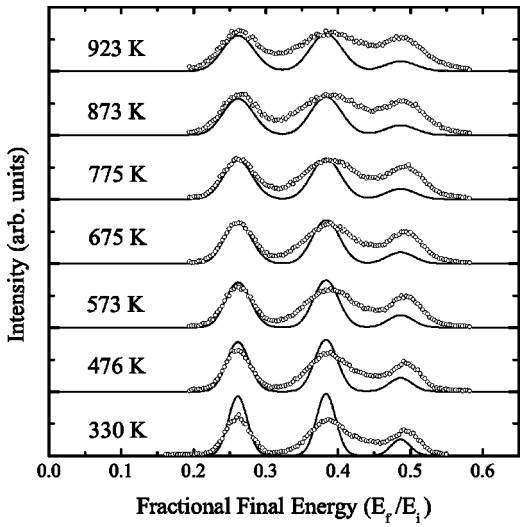

FIG. 2. Energy-resolved intensity spectra for an incident energy $E_i = 154$ eV and several different temperatures as marked. The experimental data are shown as points and the solid curves are the calculations with M_c increased by 5% and with $\theta_{q,D}$, $\theta_{q,T}$, and $\theta_{r,T}$ each increased by 15%.

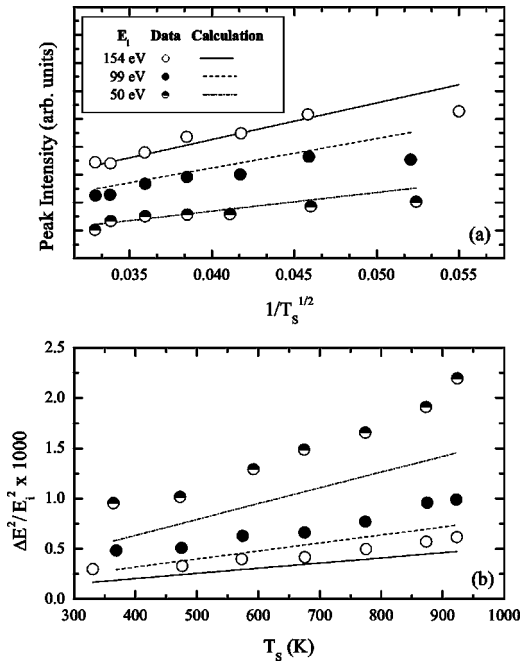

FIG. 3. *Single Scattering Trajectory*: The (a) peak intensity and (b) mean-squared width plotted as a function of $T_S^{-1/2}$ and T_S, respectively, for the three indicated incident energies. The symbols and lines correspond to the experimental data points and calculated results, respectively. The error associated with the experimental points is on the order of the displayed symbol sizes.

obtained for K^+ incident on a Cu crystal where the Cu atomic mass has been increased by 5%. In these calculations, we have also modified the intermediate scattering angles for the MS contributions, increasing them by 15% over the values shown in Table I. These slightly increased angles are closer to the angles obtained by tracing straight lines between the substrate atoms and thus are closer to the initial directions taken by the K^+ projectiles just after the intermediate collisions than the average angle obtained from the classical trajectory simulations. As one can see from Fig. 2, these modifications improve the quantitative agreement of the calculations with the experimental spectra.[37] Furthermore, the data in the figure show that there is no discernible temperature dependence in the peak positions, a result that is consistent with the classical theory.

B. Peak intensities and widths

The theoretical model presented in Sec. III predicts that the peak intensity and squared width should vary linearly as a function of $T_S^{-1/2}$ [Eq. (8)] and T_S [Eq. (4)], respectively, for single scattering trajectories. These predicted temperature dependences also apply approximately to the more complex trajectory types, since single scattering terms are convolved to model these trajectory types. Here we compare these predictions with the experimental data for K^+ scattering.

1. Single scattering

In Fig. 3(a) the experimental peak intensity (symbols) is plotted for the SS trajectory at incident energies of 50, 99, and 154 eV as a function of $T_S^{-1/2}$. Also plotted are the theoretical predictions (lines) for the SS trajectory type at these incident energies. By plotting the intensity as a function of $T_S^{-1/2}$ the predicted dependence on temperature clearly manifests itself for the calculated results. Comparing the calculation to the experimental result, one sees that the two results agree well at high temperatures. The lowest temperature experimental data, however, show a distinct departure from the calculated result. This offset is magnified by the fact that each set of intensity values have been normalized to the calculation at 675 K.

The remarkable linearity seen in the experimental peak intensity data as a function of $T_S^{-1/2}$ is particularly interesting. It demonstrates that the K^+ SS trajectory, under these experimental conditions, is most accurately described by the discrete scattering model discussed in Sec. III. This can be contrasted with the temperature dependence observed in previous measurements made for the scattering of atomic Ar from molten Ga and In surfaces.[38] In that work, the temperature dependence of the intensity was found to be approximately T_S^{-1}, a result that is intermediate between the discrete or $T_S^{-1/2}$ dependence and the $T_S^{-3/2}$ dependence one obtains for scattering from a flat, uncorrugated surface.[39] One should also note that previous measurements made using Na^+ under similar experimental conditions were unable to address the discrete scattering prediction for the temperature dependence of the peak intensity because of neutralization effects.[2,9] The scattering of K^+, however, is not sensitive to temperature-dependent neutralization effects as we stated earlier.[25]

In Fig. 3(b) we plot the mean square deviation as a function of T_S for the SS trajectory. The predicted linear dependence is clear for the calculated results, and the experimental data are in relatively close agreement with these results at the two higher incident energies. The experimental data at 50 eV also exhibit a linear trend, which is consistent with the pre-

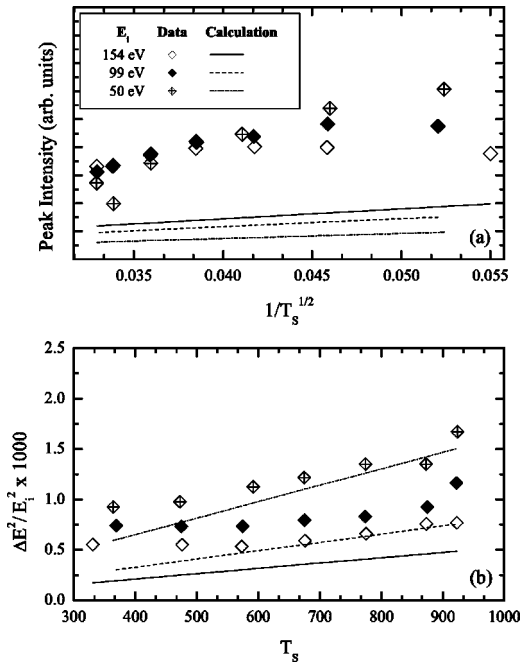

FIG. 4. *Double Forward Trajectory*: The (a) peak intensity and (b) mean-squared width plotted as a function of $T_S^{-1/2}$ and T_S, respectively, for the three indicated incident energies. The symbols and lines correspond to the experimental data points and calculated results, respectively. The error associated with the experimental points is on the order of the displayed symbol sizes.

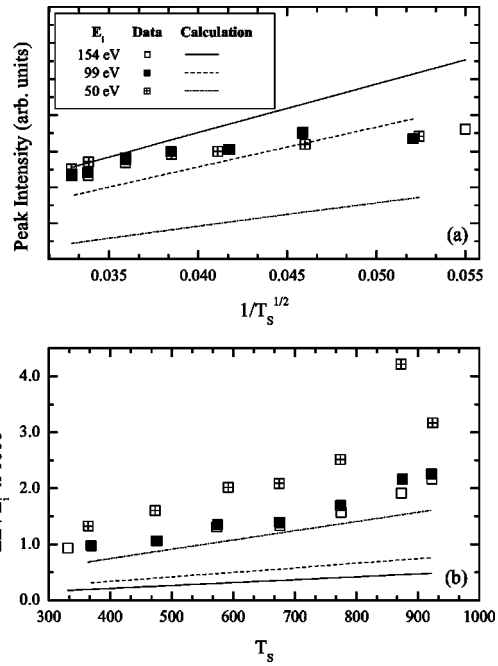

FIG. 5. *Multiple Scattering Trajectory*: The (a) peak intensity and (b) mean-squared width plotted as a function of $T_S^{-1/2}$ and T_S, respectively, for the three indicated incident energies. The symbols and lines correspond to the experimental data points and calculated results, respectively. The error associated with the experimental points is on the order of the displayed symbol sizes.

diction of Eq. (4), but they are offset from the calculated result. This quantitative difference could be attributed to temperature-independent peak broadening arising from processes other than the phonon exchange mechanism included in the present theory. Examples of additional process might be atomic excitations, electron-hole pair creation, surface and bulk plasmon creation, and charge transfer. A similar but significantly larger deviation was also observed for the case of Na^+ scattering from Cu(001).[2,16]

2. Double forward and multiple scattering

In Figs. 4(a) and 5(a) the peak intensities are plotted as a function of $T_S^{1/2}$ for the DF and MS trajectory types, respectively, at incident energies of 50, 99, and 154 eV. Also plotted are the theoretical predictions for these two trajectory types. In both sets of results, significant differences are observed between the experimental data and the calculations. Looking first at the DF results, it is clear that unlike the results for the SS trajectory type, there is a large offset between the experimental and calculated peak intensities. Noting that all of the calculations were normalized to the SS peak intensities, the offsets we observe indicate that the calculation is not reproducing the relative peak intensity that is measured for the SS and DF trajectory types. Such an offset can be accounted for in the calculation by increasing the solid angle or $\Delta\Omega$ value for the DF trajectory type. Indeed, as we discussed in Sec. III, we chose a value for the solid angle that was intermediate between that given by the Cu atomic and covalent radii. However, since one consistent $\Delta\Omega$ value is carried throughout the calculation for both DF and MS trajectory types, any adjustment would offset the calculated MS values as well. An alternative approach would be to assign independent values for the DF and MS trajectory types, but this was not attempted in the current study. Future applications of our calculation method will explore this possibility. If we focus solely on the temperature-dependent trends in the data, it is clear that there is a significant deviation from the predicted linearity at low T_S values in the 99 and 154 eV results. This is similar to the observation made for the SS trajectory type, where these higher incident energy values also deviated from linearity at low T_S values. The one trend present in the data that is consistent with the calculation is that the peak intensities approach a common value at high surface temperatures.

For the more complex MS results in Fig. 5(a), the experimental data and the predicted results also show disagreement. Although there is some quantitative agreement for the 154 eV data at high surface temperatures, all of the incident energies exhibit a linear dependence that has a smaller slope than the predicted results. Moreover, the calculations predict a large variation in intensity for the different incident energies. The data, however, exhibit a similar peak intensity at each surface temperature value that is essentially independent of the incident energy.

Significant differences between the experimental data and the calculated results are also observed for the mean square deviations of the DF and MS trajectory types, which are plotted in Figs. 4(b) and 5(b) as a function of T_S. For the DF trajectory type the experimental data at 50 eV give reasonable agreement with the calculation. The data at 99 and

154 eV, however, depart distinctly from the calculated result. In particular, the experimental data at both energies show larger mean square deviations than the calculation. As we discussed above for the SS trajectory type, this could be the result of an offset arising from additional mechanisms that are not accounted for in the present theory. However, unlike the SS trajectory type, the offset seems more severe for these two higher incident energy values. Furthermore, at low T_S values there is a clear deviation from the predicted linear trend for these incident energies. For the MS trajectory type data shown in Fig. 5(b), a large offset from the calculated result is apparent for all incident energies. However, the relative offset between the three incident energies appears to be consistent with the calculation. Also, the predicted linear trend as a function of T_S is clearly present in the experimental data.

The results shown in Figs. 4 and 5 illustrate that for these more complex trajectory types the predictions of temperature dependence that appear in our classical calculation do not agree in a straightforward way with the experimental data. For the intensities of the DF and MS trajectory types, the calculation does not correctly reproduce the relative intensity with respect to the normalized SS trajectory values. Moreover, the dependence on surface temperature is only reproduced in limited instances, with significant deviations appearing as the incident energy is increased. Similarly, quantitative offsets and deviations from linearity are observed for the mean-square deviations of these two trajectory types. It is clear that a more complex model that can more accurately describe the double and triple scattering trajectories that occur at hyperthermal and low energies is required.

C. Integrated peak intensity

The combined effects of the surface temperature on both the peak intensities and mean-square deviations can be seen in Fig. 6 which shows integrated peak intensities as a function of T_S for an incident energy of 99 eV. As we discussed in Sec. III, the calculations give results that are constant for all temperatures. The experimental data for the integrated intensity of the SS trajectory type at this energy is also constant over all temperatures with a value that agrees quite well with the calculated result. One should note that the quantitative agreement obtained for the SS trajectory type is primarily due to the fact that the peak intensity of the calculation was normalized to match the experimental data. The experimental data for DF and MS trajectory types show a slight temperature dependence as well as a significant offset from the predicted integrated intensity value. Specifically, over the measured temperature range, the integrated intensity of the DF trajectory type decreases by about 20% while that of the MS trajectory type increases by about 20%. These results simply reflect the deviations seen in the intensity and widths of the DF and MS trajectories, respectively, that was seen in Figs. 4 and 5. They are a further indication that the data for the more complex DF and MS trajectories do not completely follow the predictions of the quasi-Gaussian approximation of Eqs. (4)–(8). Similar results for the integrated peak intensities were obtained at incident energies of 50 and 154 eV.

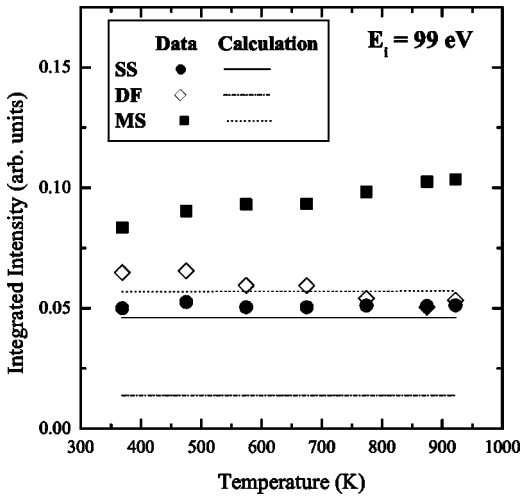

FIG. 6. Temperature dependence of the integrated peak intensity for the single scattering, double forward, and multiple scattering trajectory types at $E_i = 99$ eV. The symbols and lines correspond to the experimental and calculated results, respectively. The error associated with the experimental points is on the order of the displayed symbol sizes.

V. CONCLUSIONS

We have presented the results of an experimental and theoretical study of the scattering of singly charged potassium ions from a Cu(001) crystal surface. Energy-resolved spectra of the scattered ions were made at three different incident energies in the range $50 < E_i < 154$ eV and at surface temperatures of $325 < T_S < 925$ K. These spectra, obtained at $\theta_i = \theta_f = 45°$, show three distinct peaks, which have been identified using a classical trajectory simulation. These peaks correspond to single (SS), double forward (DF), and double (DZZ) and triple zig-zag (TZZ) scattering trajectories between the incident K^+ ions and Cu surface atoms. By operating in a regime that eliminated temperature-dependent charge exchange effects, this experiment was able to quantitatively measure the relative peak intensities as a function of surface temperature.

The behavior of the peaks in the energy resolved spectra, as functions of incident energy and crystal temperature, was analyzed with a scattering model that includes only these four scattering paths. In this model, the single scattering contribution to the intensity is expressed as a simple analytical expression while the more complex scattering trajectories are described in terms of convolutions of single scattering events. At all measured energies, the theoretical model gives reasonable quantitative agreement with the observed peak positions of all the trajectory types. The model also gives good agreement for the temperature dependence of the observed peak intensities and mean-square deviations of the SS trajectory type. The agreement observed for the SS trajectory type provides confirmation of the $T_s^{1/2}$ behavior of the mean-square deviation and the $T_S^{-1/2}$ behavior of the peak intensity predicted by the theoretical expression of Eq. (1). Significant deviations from the theoretical model are observed for the more complex DF and MS trajectory types. The level of disagreement indicates that at hyperthermal and low energies

a more complex model is required to reproduce the observed temperature-dependent trends for these trajectories.

Our results demonstrate that the single scattering of ions in this energy regime can be well explained by a classical model of discrete two-body interactions. The model, which can be written in terms of relatively simple closed-form mathematical expressions, provides certain advantages over purely numerical classical trajectory and molecular dynamics methods. For example, the simple form of this theory allows a straightforward interpretation of the response of scattered intensities to changes in initial conditions or to changes of projectile or substrate. However, our results also demonstrate that these other methods or a modification of the present method may be required to provide an accurate description of the more complex multiple-scattering trajectory types.

ACKNOWLEDGMENTS

This work was supported by the U.S. Department of Energy under Grant No. DE-FG02-98ER45704 and by the National Science Foundation under Grant Nos. DMR-0089503 and DMR-9722771. Additional support was provided by an NSF Traineeship (CES), by an NSF Research Experience for Undergraduates (REU) supplement (JP), and by the National Physical Science Consortium (JRH).

*Present address: Laboratory of Atomic and Solid State Physics, Cornell University, Ithaca, New York 14853-2501.

†Present address: Department of Physics and Astronomy, Clemson University, Clemson, South Carolina 29634.

‡Present address: Department of Chemistry, Pennsylvania State University, University Park, PA 16802.

§Present address: Woods Hole Oceanographic Institution, Woods Hole, MA 02543.

‖Deceased.

[1] B. H. Cooper and E. R. Behringer, in *Low Energy Ion-Surface Interactions, Advances in Ion Chemistry and Physics*, edited by J. Wayne Rabalais (Wiley, Sussex, 1994).

[2] C. A. DiRubio, D. M. Goodstein, B. H. Cooper, and K. Burke, Phys. Rev. Lett. **73**, 2768 (1994).

[3] D. M. Goodstein, C. A. DiRubio, B. H. Cooper, and K. Burke, Surf. Rev. Lett. **1**, 175 (1994).

[4] C. A. DiRubio, R. L. McEachern, J. G. McLean, and B. H. Cooper, Phys. Rev. B **54**, 8862 (1996).

[5] D. M. Goodstein, E. B. Dahl, C. A. DiRubio, and B. H. Cooper, Phys. Rev. Lett. **78**, 3213 (1997).

[6] K. W. Sulston and F. O. Goodman, J. Chem. Phys. **112**, 2486 (2000).

[7] F. O. Goodman and K. W. Sulston, J. Chem. Phys. **114**, 3265 (2001).

[8] C. E. Sosolik and B. H. Cooper, Nucl. Instrum. Methods Phys. Res. B **182**, 167 (2001).

[9] C. E. Sosolik, J. R. Hampton, A. C. Lavery, B. H. Cooper, and J. B. Marston, Phys. Rev. Lett. **90**, 013201 (2003).

[10] B. W. Dodson, Phys. Rev. B **36**, 1068 (1987).

[11] H. P. Kaukonen and R. M. Nieminen, Phys. Rev. Lett. **68**, 620 (1992).

[12] A. Benninghoven, F. G. Rudenauer, and H. W. Werner, *Secondary Ion Mass Spectrometry* (Wiley, New York, 1987).

[13] L. K. Verhey, B. Poelsema, and A. L. Boers, Phys. Lett. **53A**, 381 (1975).

[14] B. Poelsema, L. K. Verhey, and A. L. Boers, Surf. Sci. **56**, 445 (1976).

[15] B. Poelsema, L. K. Verheij, and A. L. Boers, Surf. Sci. **133**, 344 (1983).

[16] A. Muis and J. R. Manson, Phys. Rev. B **54**, 2205 (1996).

[17] R. L. McEachern, D. L. Adler, D. M. Goodstein, G. A. Kimmel, B. R. Litt, D. R. Peale, and B. H. Cooper, Rev. Sci. Instrum. **59**, 2560 (1988).

[18] D. L. Adler and B. H. Cooper, Rev. Sci. Instrum. **59**, 137 (1988).

[19] D. L. Adler, B. H. Cooper, and D. R. Peale, J. Vac. Sci. Technol. A **6**, 804 (1988).

[20] M. Menzinger and L. Wåhlin, Rev. Sci. Instrum. **40**, 102 (1969).

[21] D. R. Peale, D. L. Adler, B. R. Litt, and B. H. Cooper, Rev. Sci. Instrum. **60**, 730 (1989).

[22] Heatwave, Watsonville, California, 95076.

[23] C. E. Sosolik, A. C. Lavery, E. B. Dahl, and B. H. Cooper, Rev. Sci. Instrum. **71**, 3326 (2000).

[24] G. A. Kimmel and B. H. Cooper, Rev. Sci. Instrum. **64**, 672 (1993).

[25] C. E. Sosolik, Ph.D. thesis, Cornell University (2001).

[26] C. E. Sosolik, J. R. Hampton, A. C. Lavery, J. B. Marston, and B. H. Cooper (unpublished).

[27] Thomas Hecht, Ph.D. thesis, Humboldt Universität zu Berlin (1999).

[28] D. M. Goodstein, S. A. Langer, and B. H. Cooper, J. Vac. Sci. Technol. A **6**, 703 (1988).

[29] D. M. Goodstein, R. M. McEachern, and B. H. Cooper, Phys. Rev. B **39**, 13 129 (1989).

[30] C. A. DiRubio, G. A. Kimmel, and R. L. McEachern, Nucl. Instrum. Methods Phys. Res. B **64**, 49 (1992).

[31] The SS and DF trajectories have also been labeled as quasi-single (QS) and quasi-double (QD) trajectory types, e.g., in Ref. 1.

[32] A. Muis and J. R. Manson, Nucl. Instrum. Methods Phys. Res. B **125**, 332 (1997).

[33] A. Muis and J. R. Manson, J. Chem. Phys. **111**, 730 (1999).

[34] A. Sjölander, Ark. Fys. **14**, 315 (1959).

[35] J. R. Manson, Phys. Rev. B **58**, 2253 (1998).

[36] C. A. DiRubio, Ph.D. thesis, Cornell University (1993).

[37] The adjusted Cu atomic mass and MS intermediate scattering angles do not significantly alter the temperature dependence of the peak intensities, widths, or integrated intensities.

[38] W. R. Ronk, D. V. Kowalsi, M. Manning, and G. M. Nathanson, J. Chem. Phys. **104**, 4842 (1996).

[39] A. Muis and J. R. Manson, J. Chem. Phys. **107**, 1655 (1997).